Metal-Matrix Composites and Thermal Spray Coatings for Earth Moving Machines
Quarter 9 Report

Reporting Period Start Date: 01/01/03
Reporting Period End Date: 03/31/03

Authors:
D. Trent Weaver (Caterpillar)
Frank W. Zok and Carlos G. Levi (UC Santa Barbara)
Matthew T. Kiser (Caterpillar)

April 2003

DOE Award: DE-FC26-01NT41054

Caterpillar Inc.
Technical Center – E – 854
PO Box 1875
Peoria, IL 61656-1875

Materials Department
University of California
Santa Barbara, CA 93106

Metal-Matrix Composites and Thermal Spray Coatings for Earth Moving Machines
Quarter 9 Report

Table of Contents

Metal-Matrix Composites and Thermal Spray Coatings for Earth Moving Machines
Quarter 9 Report

Abstract:

In the ninth quarter, investigations in steel matrix composites focused on characterization of abrasive wear and fracture test coupons in order to gain a better understanding of the material attributes contributing to the observed behavior in each test. Both the wear and fracture work found that the performance of the carbide cermet based composites was significantly affected by the dissolution of the hard particles and the elements added in hopes of discouraging dissolution. both thrusts focused on abrasive wear characterization. In abrasive wear this led to increase matrix hardness which increased wear resistance, however the fracture toughness of the composites were significantly reduced. In contrast, the oxide based composites demonstrated good fracture characteristics and the oxide particles provided superior protection to the high stress gouging wear imparted by pin-abrasion testing.

For the thermal spray coating effort, modified coatings and fusing parameters were explored on simulated components. Significant improvements appear to have been achieved, and are demonstrated in the lack of observable cracking in the coatings. The abrasive wear characteristics of these components will be explored in the 10th quarter.

An overview of the progress during the 9h quarter of this project is given below. Additional research details are provided in the limited rights appendix to this report.

Experimental

Steel Matrix Composites

Microstructural and mechanical characterization were performed on two groups of particle-reinforced steel matrix composites, for the purpose of assessing their utility in abrasion-resistant structures. In addition, coupons from pin-abrasion tests conducted at DOE Albany Research Center on these same material were analyzed to understand the mechanism leading to the observed wear trends. All composites comprised a 1045 steel matrix. The first group was reinforced with WC/Co particles. Two strategies were used to enhance wetting and infiltration: (i) small additions of a Mo-Fe-B (MFB) particles to the particle preform, and (ii) ball milling of the WC/Co particles with small amounts of FeB prior to preform fabrication and melt infiltration. These composites were produced by pressure casting at Caterpillar. The second group contained either spherical alumina or angular alumina/zirconia particles. No special efforts were made to enhance melt infiltration. Infiltration was accomplished using a hot isostatic press (HIP), configured to emulate squeeze casting, at UCSB. All specimens were normalized for prior to testing.

SEM micrographs of cross-sections through these composites as well as the neat 1045 steel matrix are shown in Figures 1–5. For both composites containing the WC/Co particles, there was significant dissolution of the particles by the steel (Figures 2 and 3). In addition to the presence of individual WC grains in the surrounding steel (e.g. Figures 2(e) and (f)), Fe levels in excess of 20% were detected within the particles at distances of a few hundred microns from the apparent

particle/matrix interface (see, for example, the light gray phase, about 300-400 μm thick, around the particle in Figure 2(c)). The matrix microstructures differed significantly from the ferrite/pearlite structure characteristic of the neat matrix. Due to the dissolution of the WC grains and the added FeB or MFB phases, a significant fraction of carbides formed upon solidification. In addition, the matrix contained very little ferrite and was comprised of either very fine pearlite or bainite.

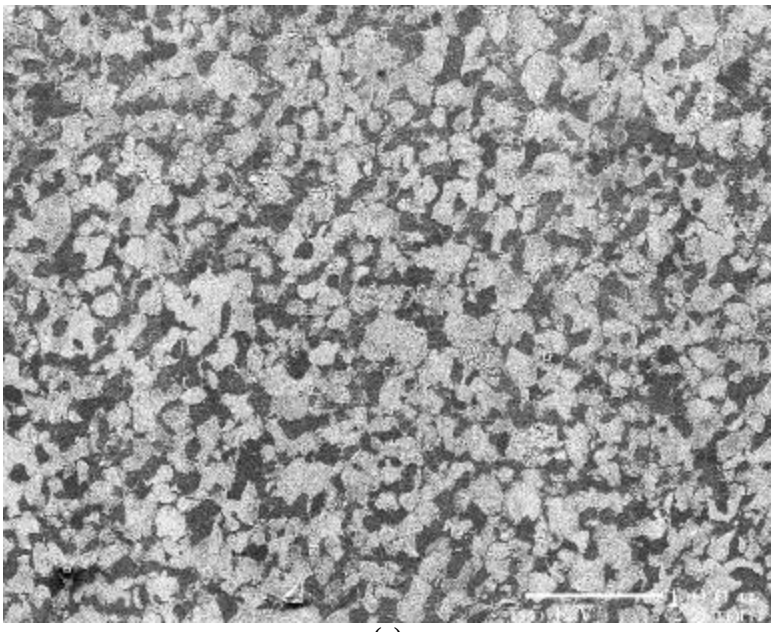

(a)

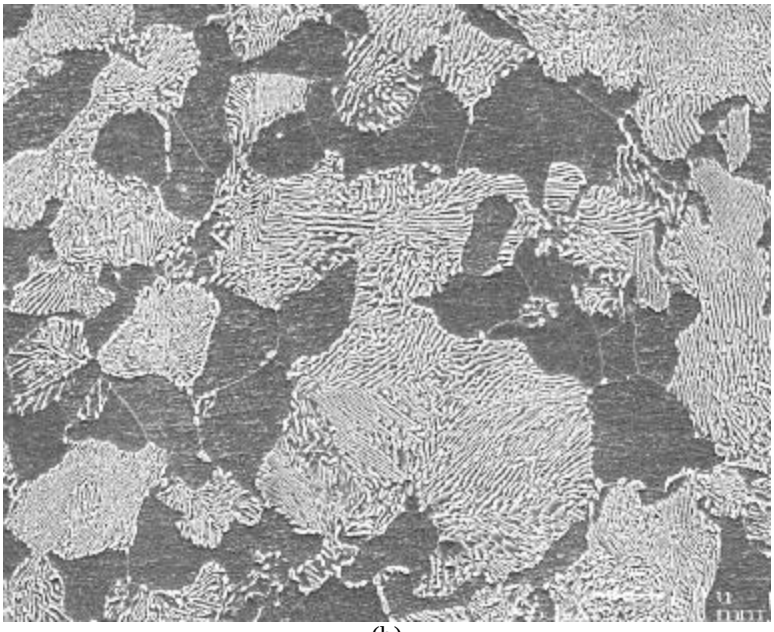

(b)

Figure 1 SEM micrographs of the neat 1045 steel matrix after normalization, showing the expected ferrite/pearlite microstructure.

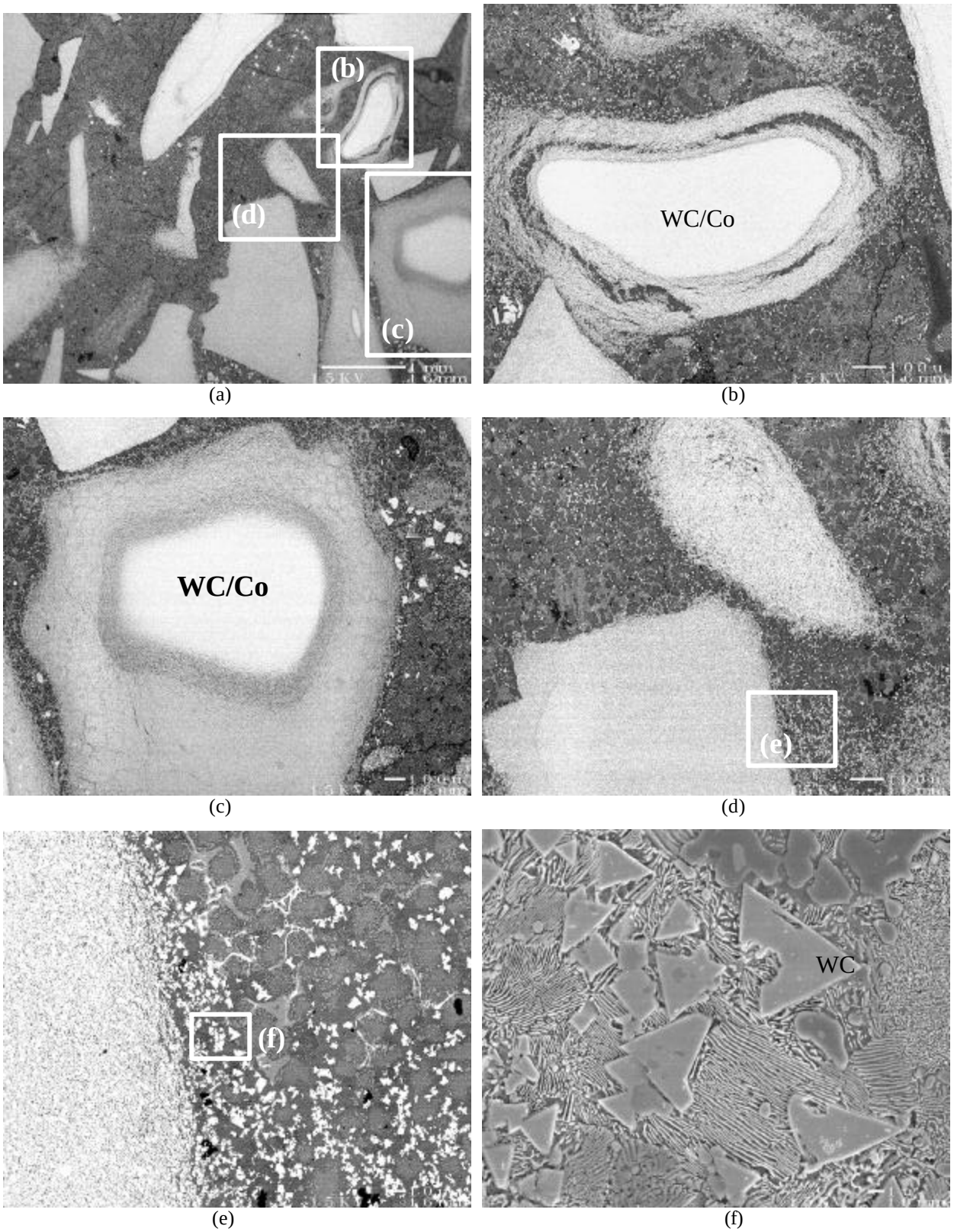

(a) (b) (c) (d) (e) (f)

Figure 2 SEM micrographs of the composite with FeB-WC/Co particles. Note the extensive dissolution of the WC/Co.

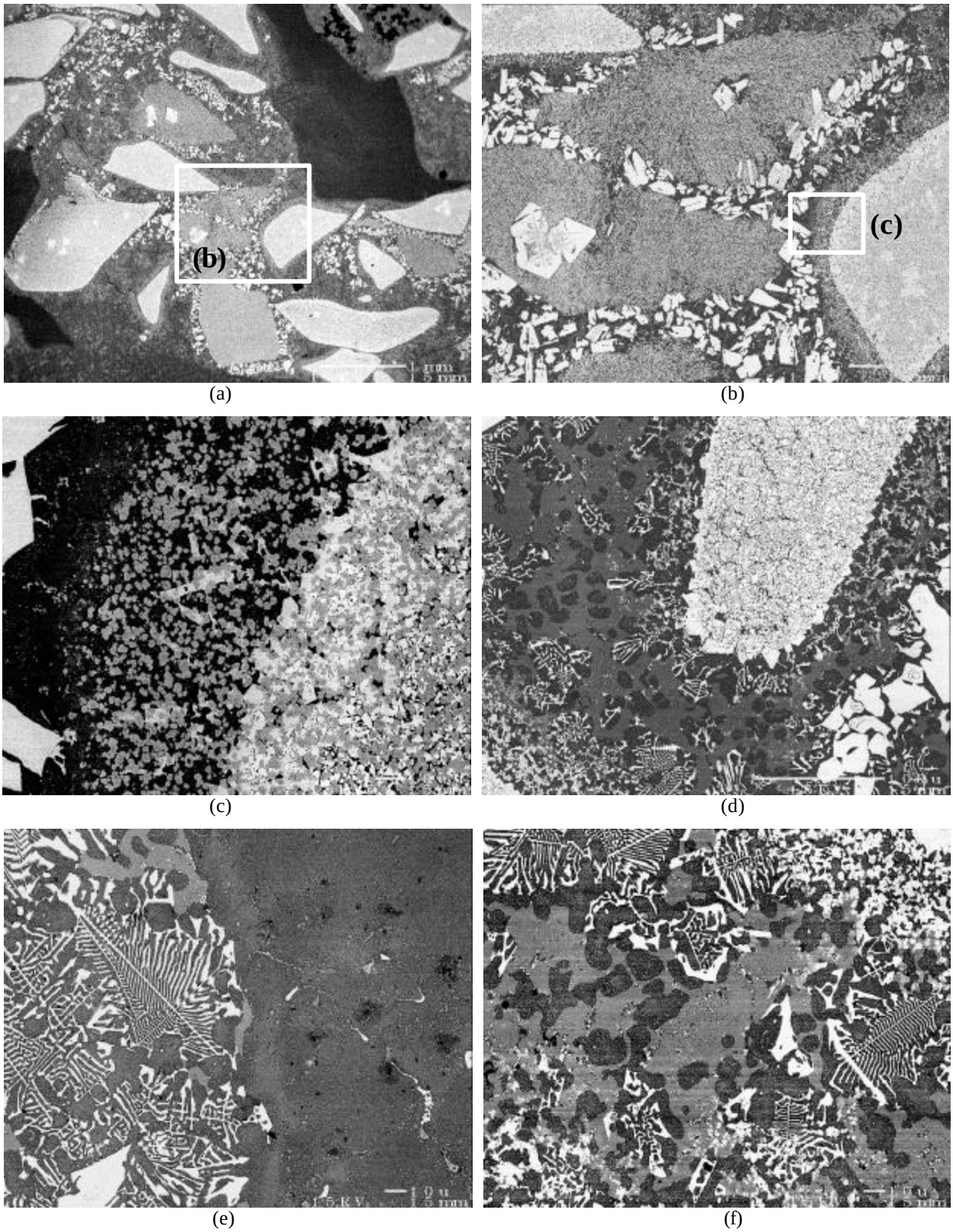

Figure 3 SEM micrographs of the composite with MFB-WC/Co particles. Note the dissolution of the WC/Co and the formation of unidentified matrix phases.

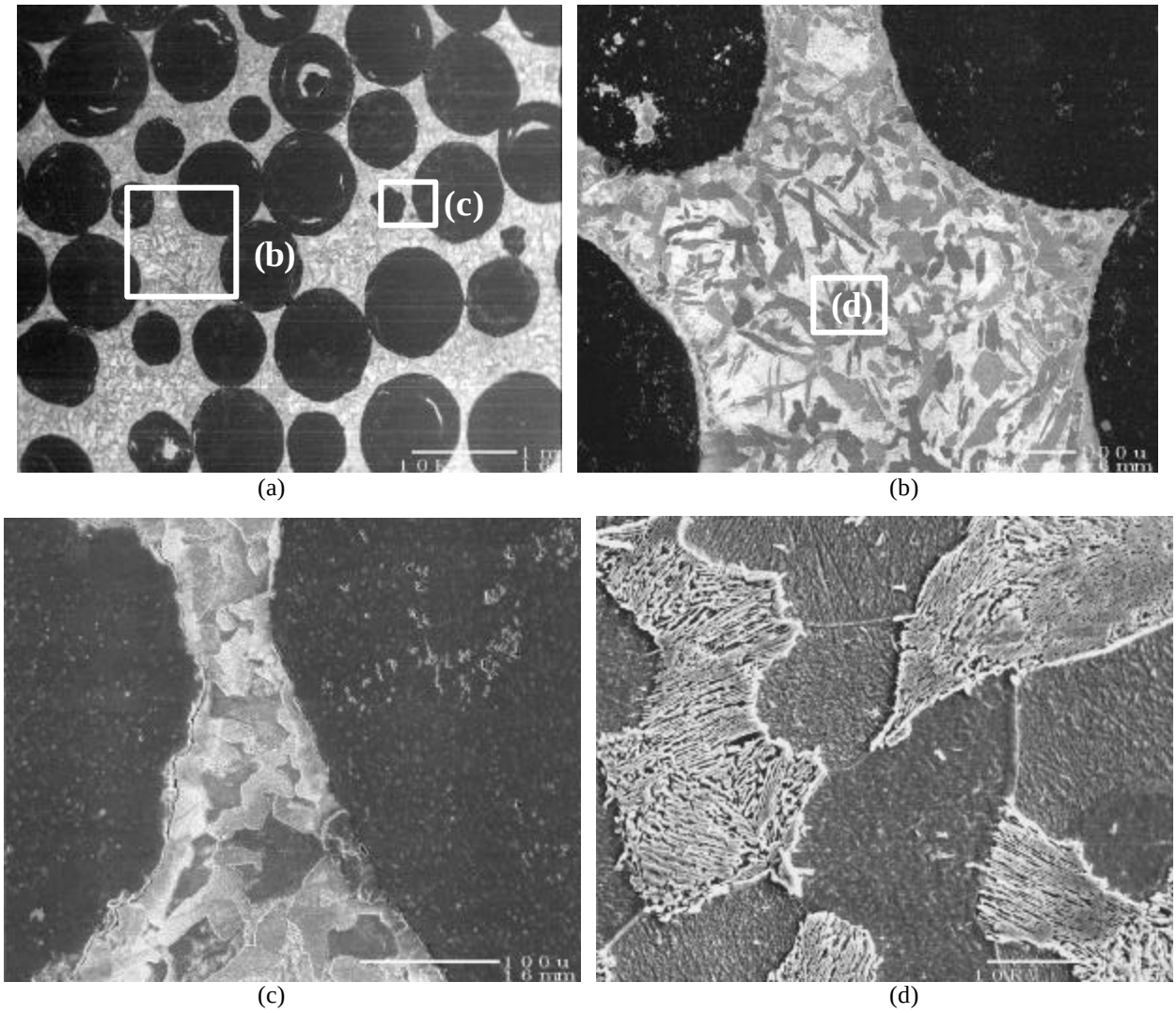

Figure 4 SEM micrographs of the composite with spherical alumina particles, showing (a) uniform distribution of particles, (b,c) distinct interfaces at the steel/particle boundary without particle dissolution, and (d) ferrite/pearlite microstructure within the matrix, similar to that of the neat material (Figure 1).

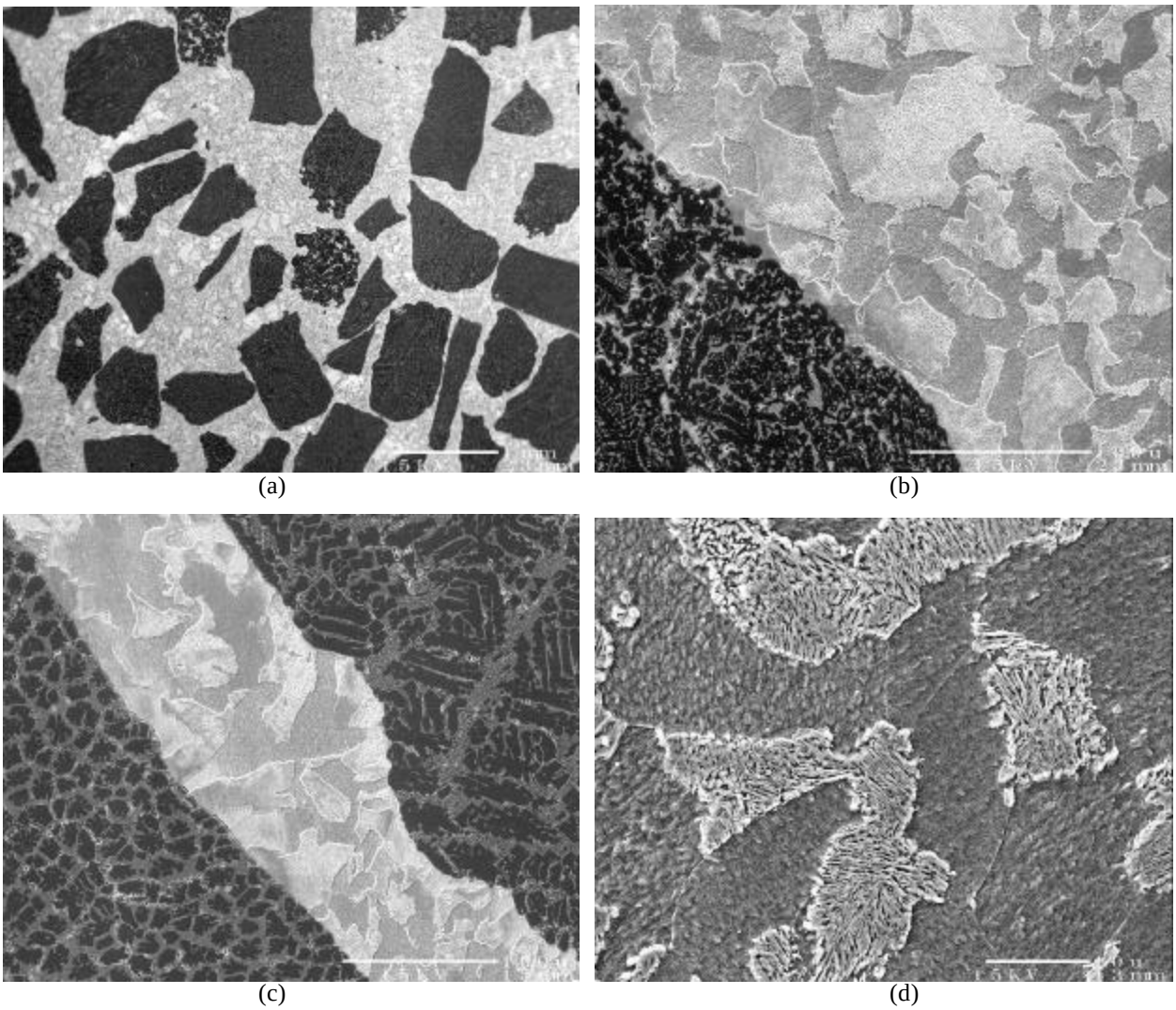

Figure 5 SEM micrographs of the composite with alumina-zirconia particles, showing similar features to that in the alumina-containing composite, notably: (a) uniform distribution of particles, (b,c) distinct interfaces at the steel/particle boundary without particle dissolution, and (d) ferrite/pearlite microstructure within the matrix.

There was no significant interaction between the phases in the composites containing either alumina or alumina-zirconia particles (Figure 4 and 5). The particles were uniformly distributed throughout the matrix (Figures 4(a) and 5(a)). The interfaces appeared distinct, without obvious dissolution of the particles or other chemical interactions (Figures 4(b, c) and 5(b, c)). Furthermore, the matrix exhibited a ferrite/pearlite microstructure, essentially the same as that of the neat alloy (compare Figures 4(d) and 5(d) with Figure 1). The only detectable interaction was in the form of trace amounts (about 1%) of Zr in the matrix in the composites containing alumina-zirconia particles. Furthermore, there was some impregnation of the melt into the pores within the latter particles. This feature is expected to enhance interface integrity through mechanical interlocking.

The effects of particle dissolution and chemical interactions with the FeB and MFB additions were manifested in significant increases in matrix hardness relative to the neat material (Figure 6). The matrix hardness in the MFB containing materials was about 5 times that of the neat steel; in the FeB material, it was more than twice as high. By contrast, both the alumina and alumina-zirconia containing composites exhibited hardness levels that were the same as that of the neat matrix, within the experimental scatter. This correlation is consistent with the noted similarities in the matrix microstructures.

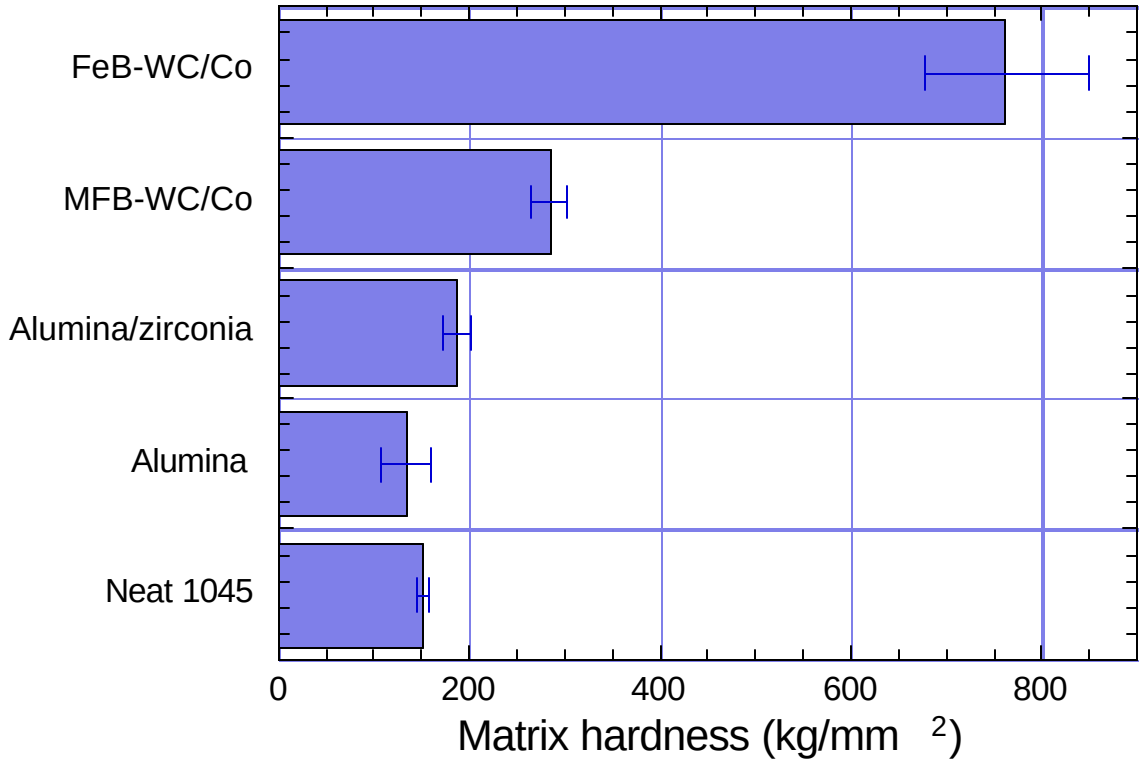

Figure 6 Summary of average matrix hardness within composites and of neat 1045 steel.

The mechanical properties of the composites were characterized using unnotched and notched bend specimens, each about 10 mm x 10 mm in cross-section and with notches of half the depth. Test coupons from the pin-abrasion test were examined using optical and SEM microscopy in an effort to understand the abrasive wear mechanisms. Coupon wear surfaces were first examined in an SEM and then were metallographically mounted, ground and polished to reveal a cross section of the wear surfaces.

Thermal Spray Coatings

Fusing of 16 functionally-graded material (FGM) coatings, was accomplished using the plasma arc lamp at Oak Ridge National Laboratory (ORNL). All coatings were designed with lower layers that metallurgically bond to the underlying substrate and absorb solidification and coefficient of thermal expansion mismatch stresses, while the upper layer(s) remain very hard and wear resistant. These coatings were deposited onto as-formed steel tubes, consistent with a component which experiences severe abrasive wear.

Results and Discussion

Steel Matrix Composites

The results from the notched and unnotched bend tests are shown in Figure 7. In the unnotched configuration, the WC/Co composites exhibited high strength (500-700 MPa) (Figure 7(a)). The FeB containing composite fractured catastrophically, whereas the one treated with MFB showed a more significant post load-maximum "tail" in the load-displacement curve. The alumina and alumina-zirconia containing composites exhibited a lower peak stress but a subsequent "graceful" failure.

In the notched condition, the alumina-zirconia material displayed the best performance. Its strength was on par with the two WC/Co composites (300–400 MPa), and higher than that of the alumina composite (about 200 MPa). Furthermore, it exhibited the highest work of fracture: almost an order of magnitude greater than that for the WC/CO materials (Figure 8).

SEM observations of the fracture surfaces were broadly consistent with the mechanical measurements. Both of the WC/Co materials displayed planar fracture surfaces and extensive cleavage cracking within the matrix (Figures 9 and 10). The alumina composites failed by interface debonding followed by local plastic stretching of the intervening matrix ligaments (Figure 11(a)). These features are consistent with the low strength and the extended tail in the notched load-displacement response (Figure 7(b)). The alumina-zirconia composite failed by particle cracking followed by deformation of the matrix. Upon comparing matching fracture surfaces, there was evidence of steel within the fractured particles; see, for example, the particles denoted 3 and 4 in Figure 12.

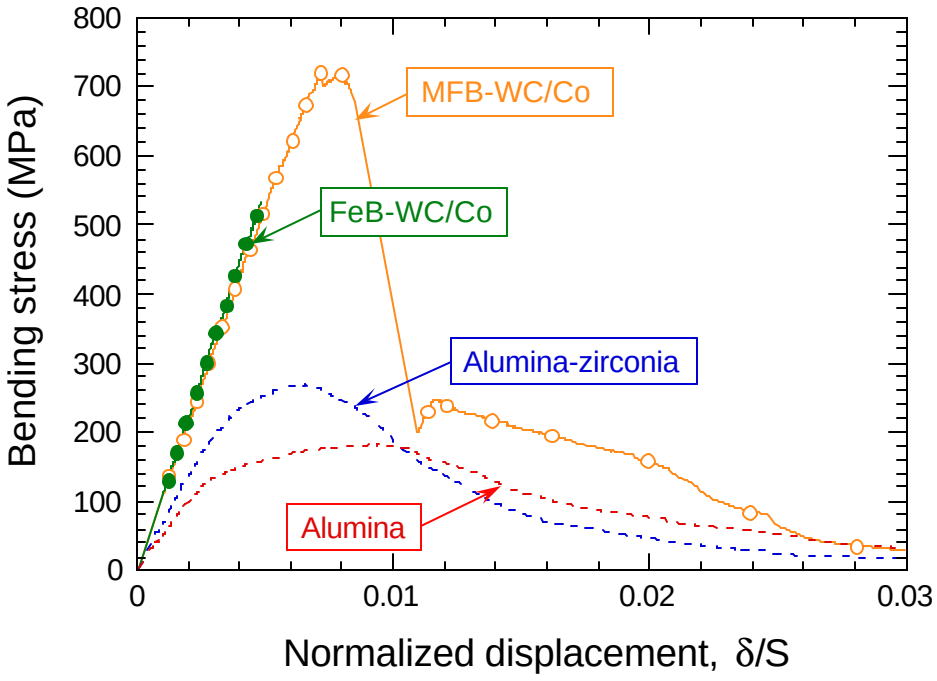

(a)

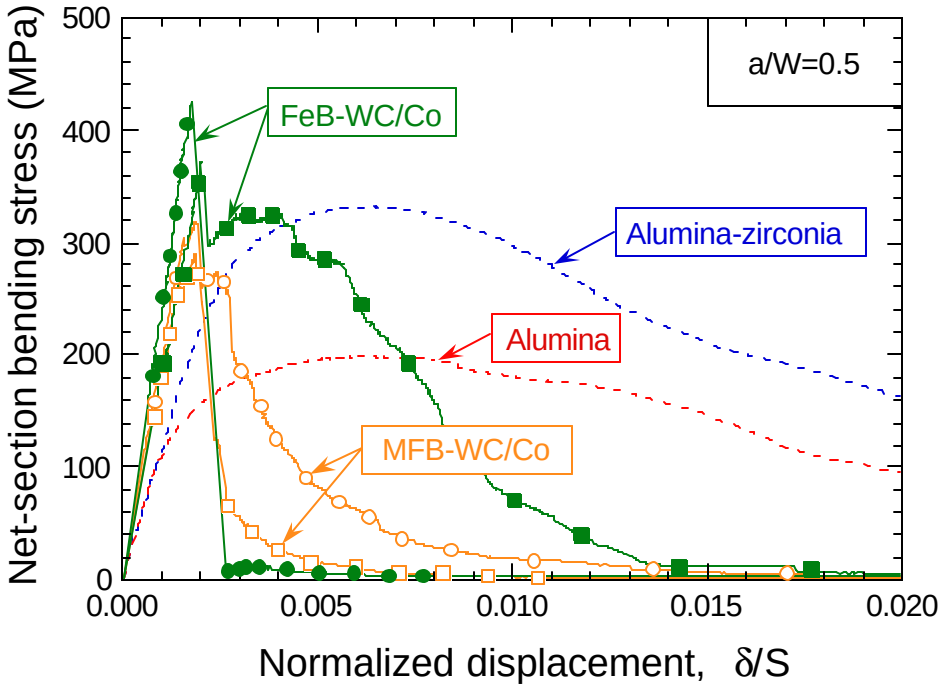

(b)

Figure 7 (a) Unnotched and (b) notched bending response of the four composites. (S is span length)

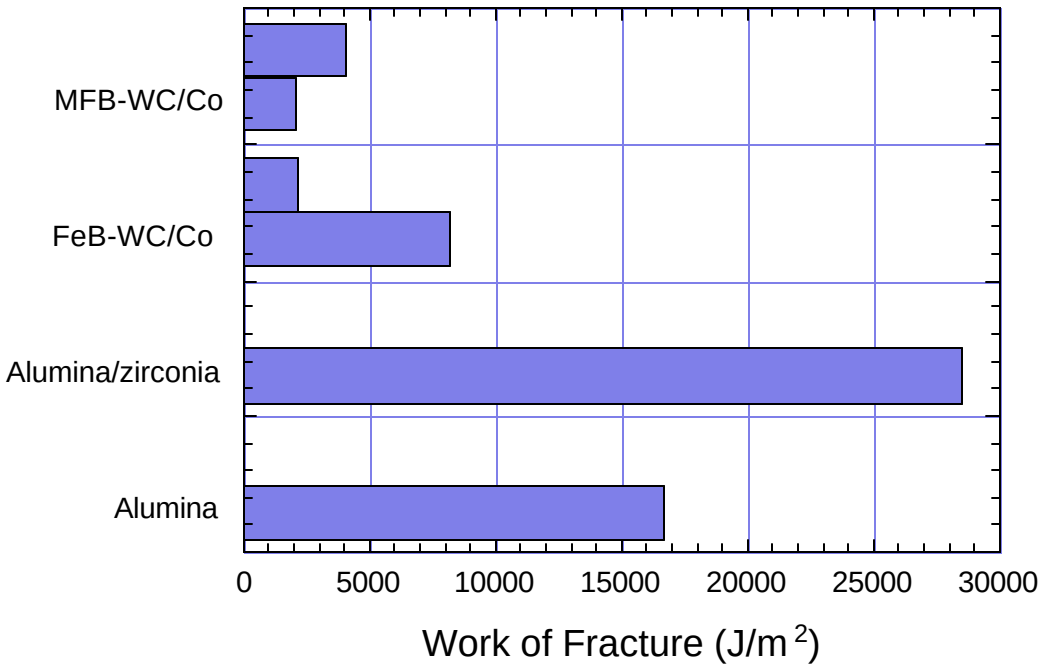

Figure 8 Work of fracture obtained from area under the notched load-displacement curves.

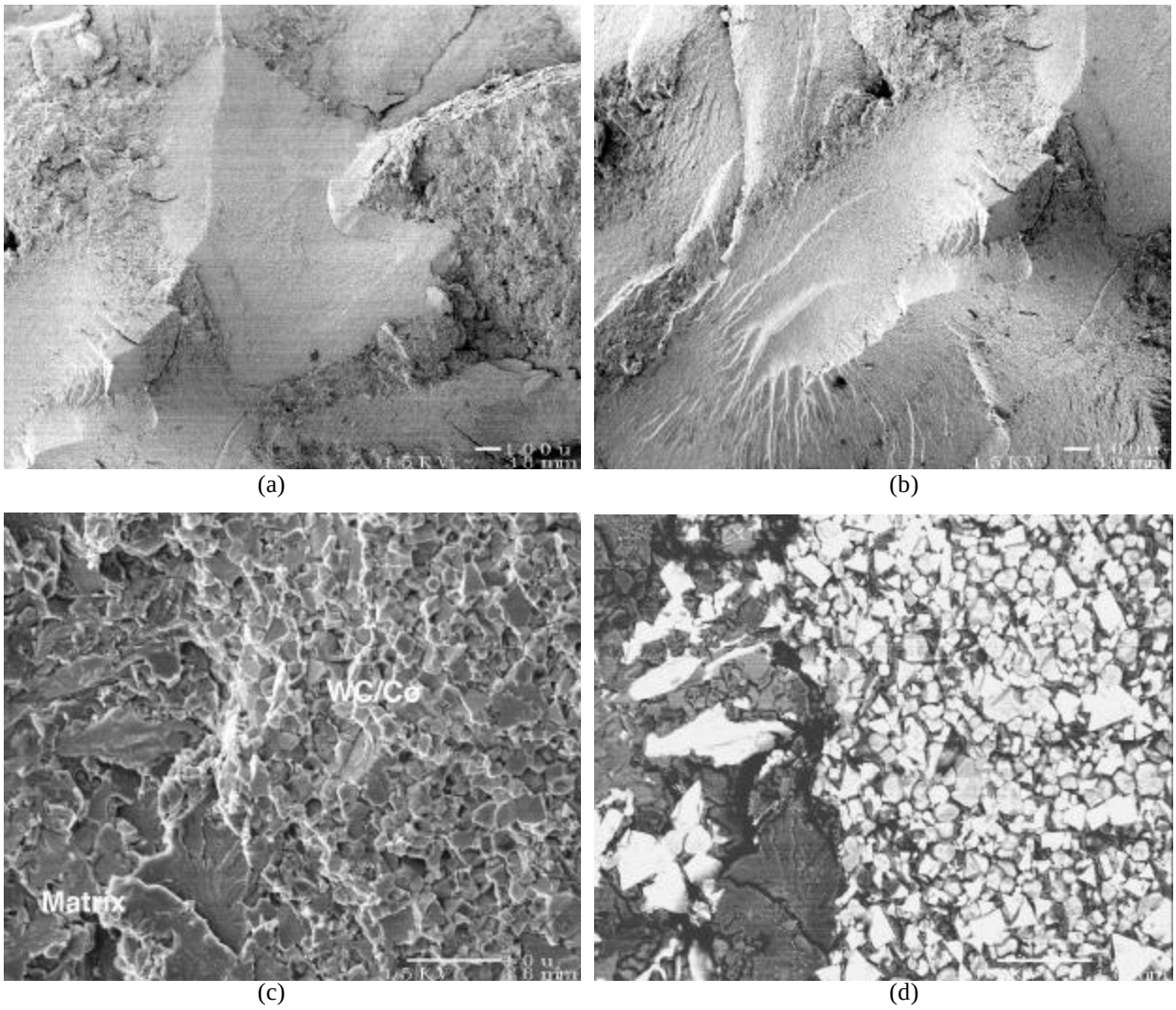

Figure 9 Fracture surfaces of the FeB-WC/Co containing composites. (c) and (d) are of the same region, in backscatter and secondary electron imaging modes, respectively. Note the cleavage facets in the matrix region of (c).

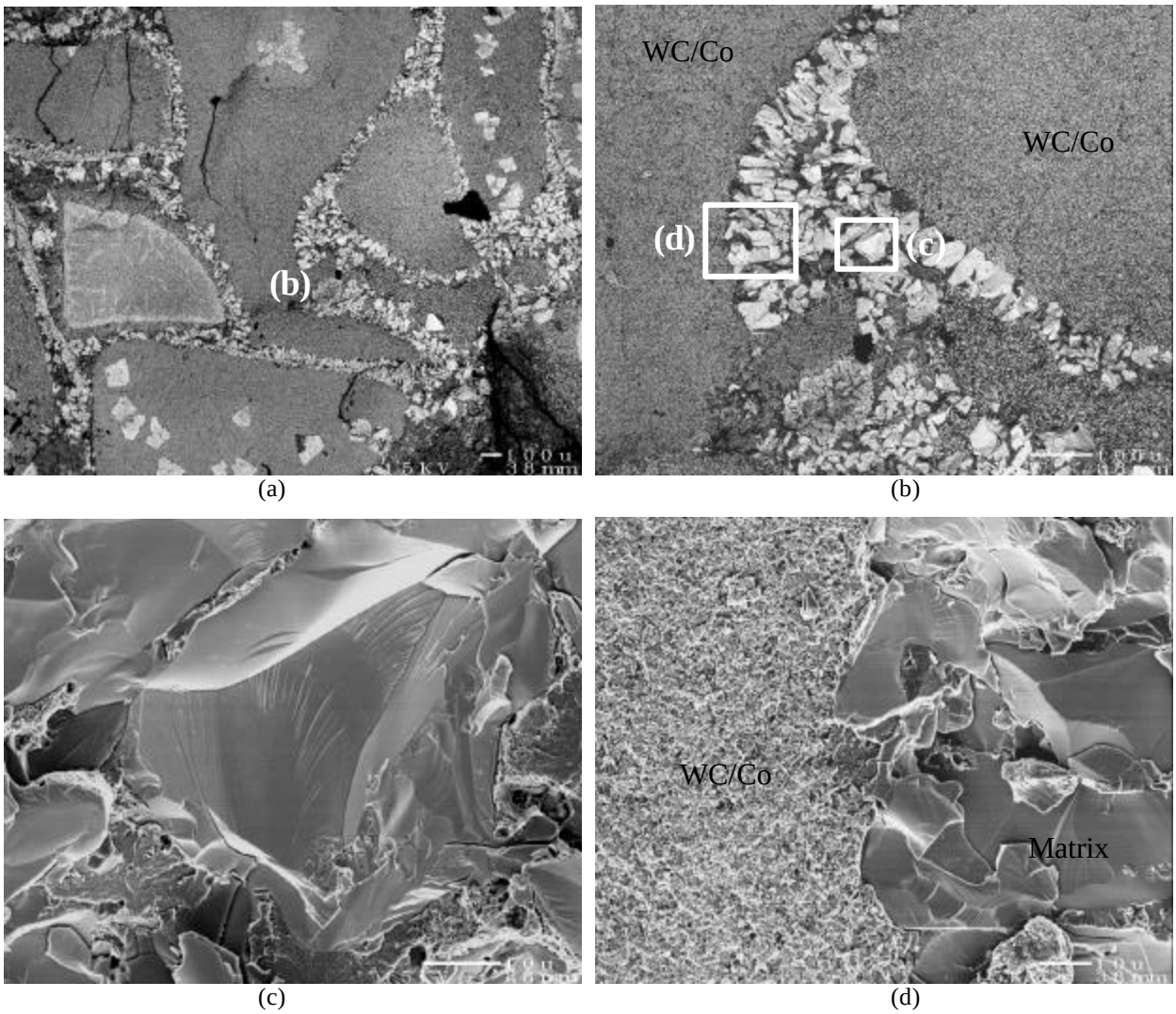

(a) (b) (c) (d)

Figure 10 Fracture surfaces of the MFB-WC/Co containing composites at progressively increasing magnifications. Matrix fracture occurs predominantly by cleavage, as illustrated in (c) and (d).

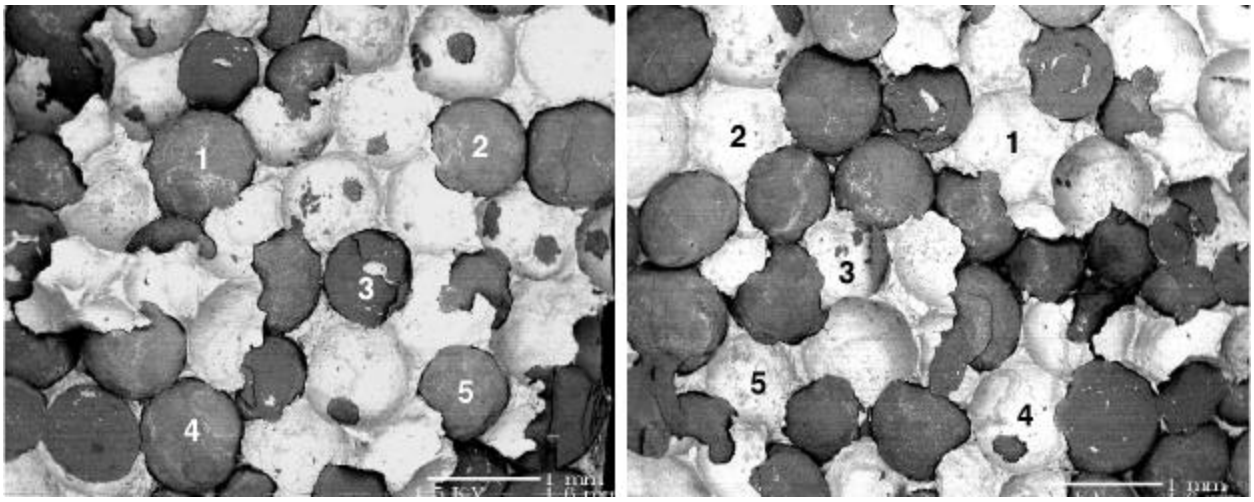

Figure 11 Matching fracture surfaces of the alumina containing composite, viewed in backscatter electron imaging mode. The numbers correspond to matching regions on the two fracture surfaces. The dark regions are alumina and the light regions are steel.

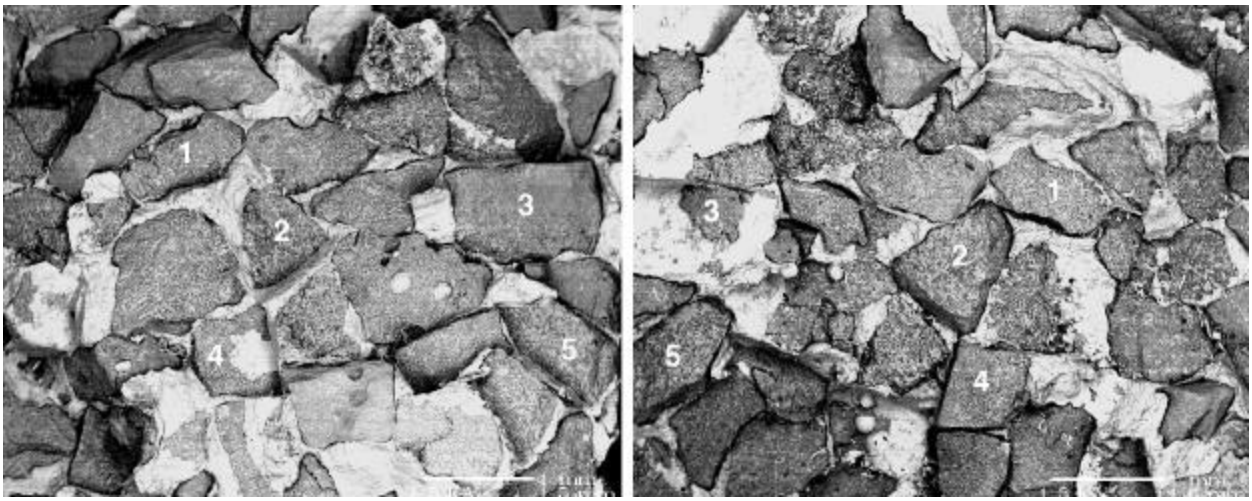

Figure 12 Matching fracture surfaces of the alumina-zirconia containing composite, viewed in backscatter electron imaging mode. The numbers correspond to matching regions on the two fracture surfaces. The dark regions are alumina-zirconia and the light regions are steel. Most particles fail by fracture. The matrix "patches" on particle 4 on the left and particle 3 on the right are a result of steel infiltration into the particles.

Abrasive wear results were presented in the Quarter 8 report and a summary of the results is provided again for reference in Figure A3. Figure 13 shows that the neat matrix displayed relatively deep scratches, with material being removed along with the occurrence of a significant amount of plasticity in both the ferrite and pearlite phases (Figure 13(b)).

The wear processes for the WC/Co composites are shown in Figures 14 and 15. The particles are observed to be raised above the plan of the matrix and are therefore wearing at a slower rate than the matrix, thus reducing the overall wear rate of the composite by providing some protection to the matrix. In contrast to the neat matrix, only shallow scratches are observed in the matrix of the WC/Co based composites and no significant subsurface matrix deformation is observed (Figures 14(e), 14(f), 15(e) and 15(f)). This is a result of the relatively high hardness of the matrix in these composites (Figure 6) and the high fraction of very hard carbides in the matrix which provide further wear resistance. Due to the carbide fraction in the matrix, the matrix wear process is likely dominated by microfracture of the carbides and localized plastic flow of the metallic matrix. The WC/Co particles appear to be worn by both scratching wear in the case of fine grain WC/Co particles (Figure 14 (c) and (d)) and grain plucking in the case of coarse grain WC/Co (Figure 15 (c) and (d)).

In the alumina and alumina-zirconia composites the particles provided substantial wear protection to the matrix (Figures 16 and 17) In these composites, the matrix was worn by a similar process to the neat matrix, given that they are of the same structure (Figures 16(e), 16(f), 17(e) and 17(f)). The scratches appear to be more shallow than those in the neat matrix, likely due to the protection provided by the particles. No scratches are observed on the particles. Particle wear mechanism appear to be primarily a result of microfracture and grain plucking (Figures 16(c), 16(d), 17(c) and 17(d)).

Thermal Spray Coatings

All coatings responded well to the arc lamp processing in terms of dimensional stability. In contrast to tubes that were internally water-cooled during fusing and reported on previously, circumferential and longitudinal coating cracking was not prevalent. Only one coating exhibited circumferential cracks that could be resolved by the unaided eye. This was likely the result of incomplete fusing of the coating due to a lower arc lamp current fusing pass than was used with the other specimens.

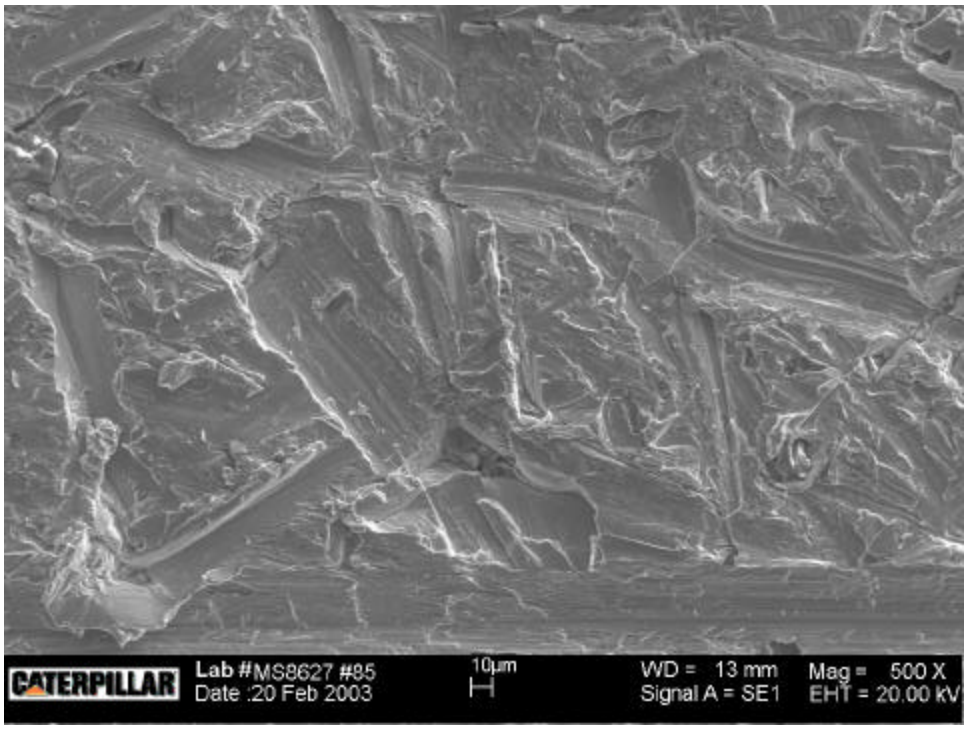

(a)

(b)

Figure 13 Pin abrasion of neat matrix. (a) SEM image of wear surface showing deep gouges and extensive plastic flow. (b) Optical image of the cross section of a scratch showing localized plastic flow revealed though deformation of pearlite grains.

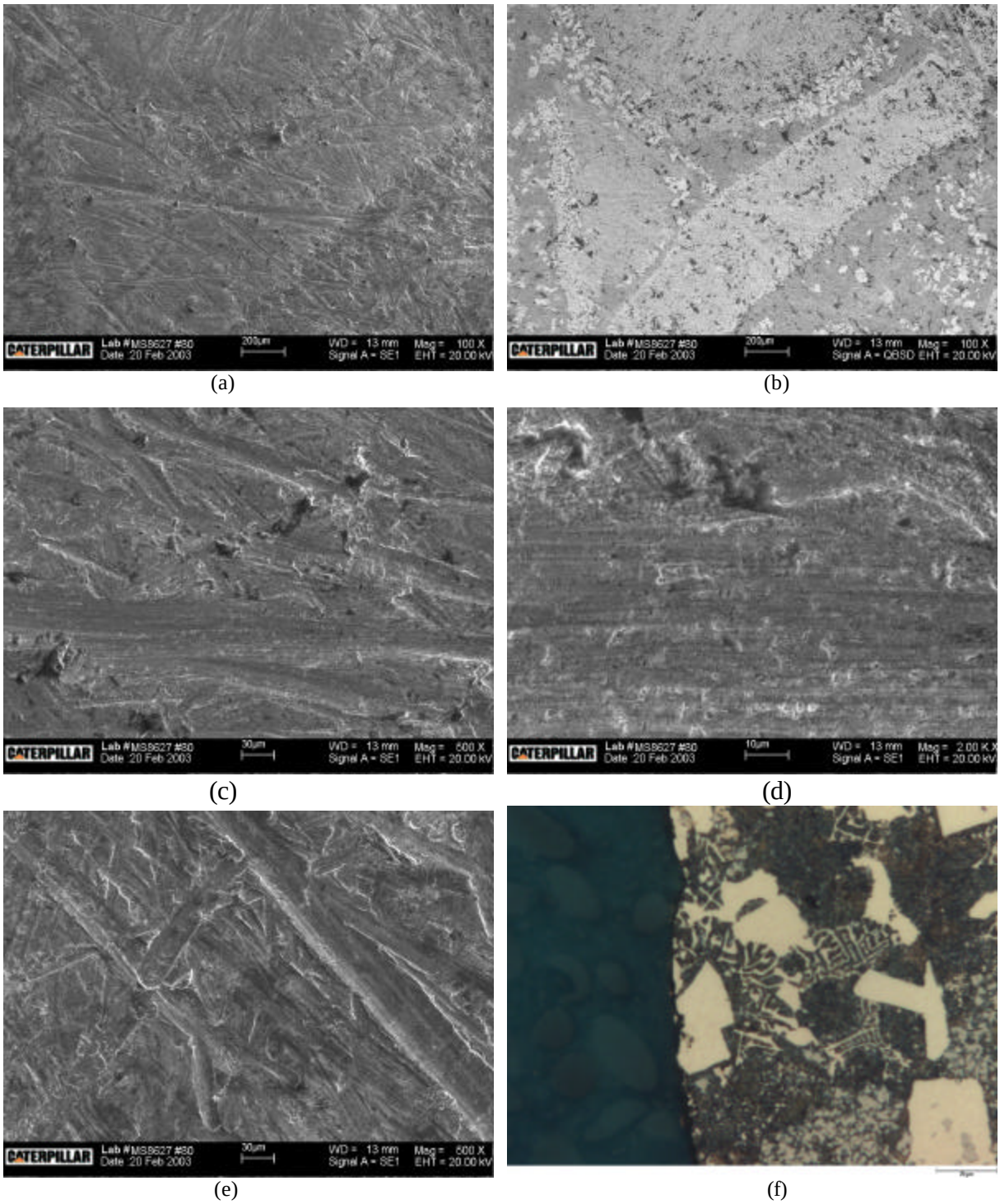

Figure 14 Wear processes in Fe-B coated WC/Co composite where (a) and (b) show the general wear process where the hard particles (distinguishable in the backscattered SEM image shown in (b) as the light-colored phase) are providing some protection to the matrix, but are also experiencing some gouging abrasion, more closely shown in (c) and (d). The matrix (e) displays shallower scratches than seen in the neat matrix, largely due to the protection provided by the carbides in the matrix (light phase in (f)).

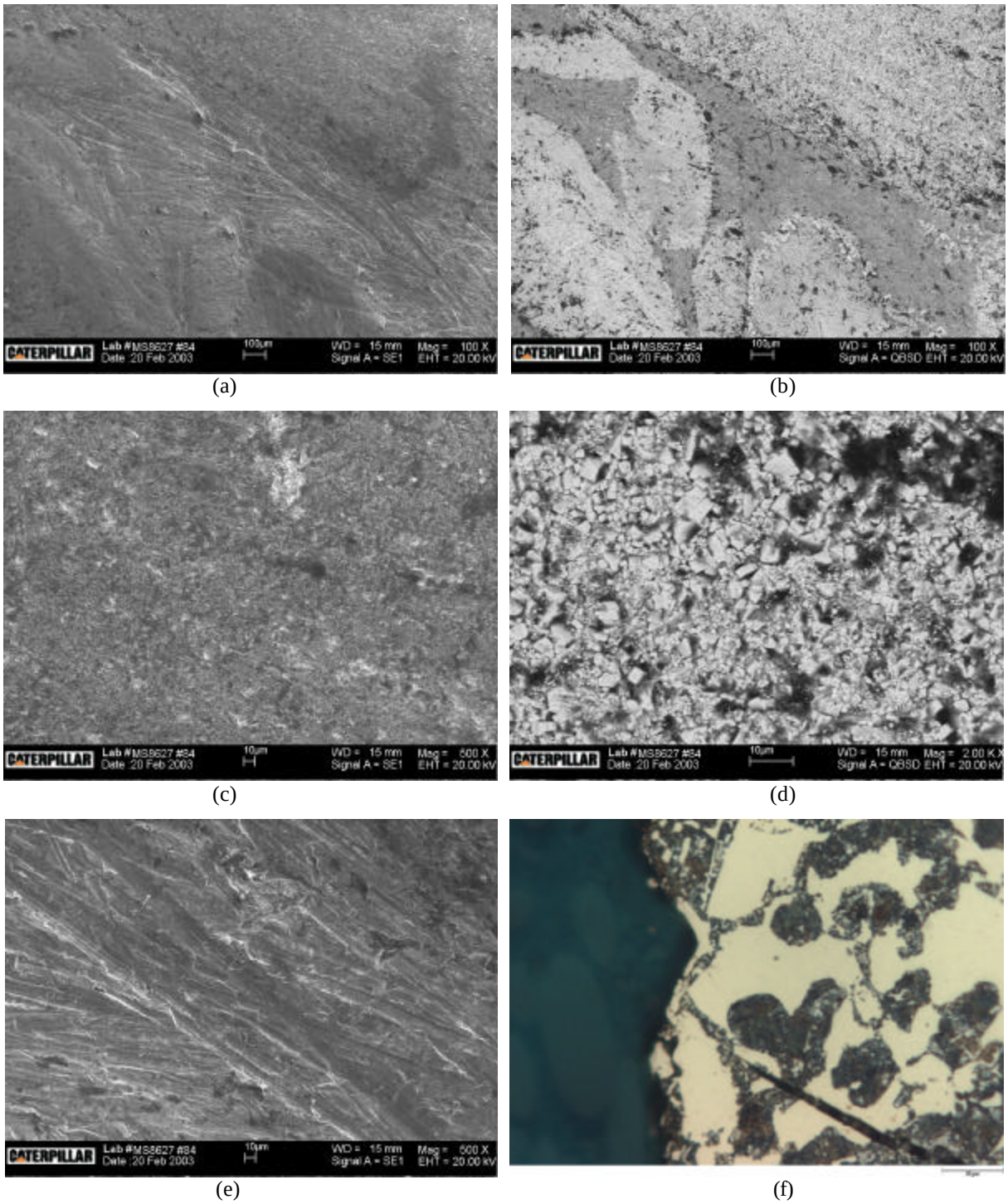

Fig. 15 WC/Co + MFB composite where (a) and (b) show the general wear process with the hard particles (distinguishable in the backscattered SEM image shown in (b) as the light-colored phase) providing some protection to the matrix. In contrast to the case shown in Fig. 14, the WC/Co particle examined does not display any clear scratches (c). Instead the particles appear to be wearing by a progressive erosion of the cermet matrix and grain plucking (d). The matrix (e) displays shallower scratches than seen in the neat matrix, largely due to the protection provided by the carbides in the matrix (light phase in (f)).

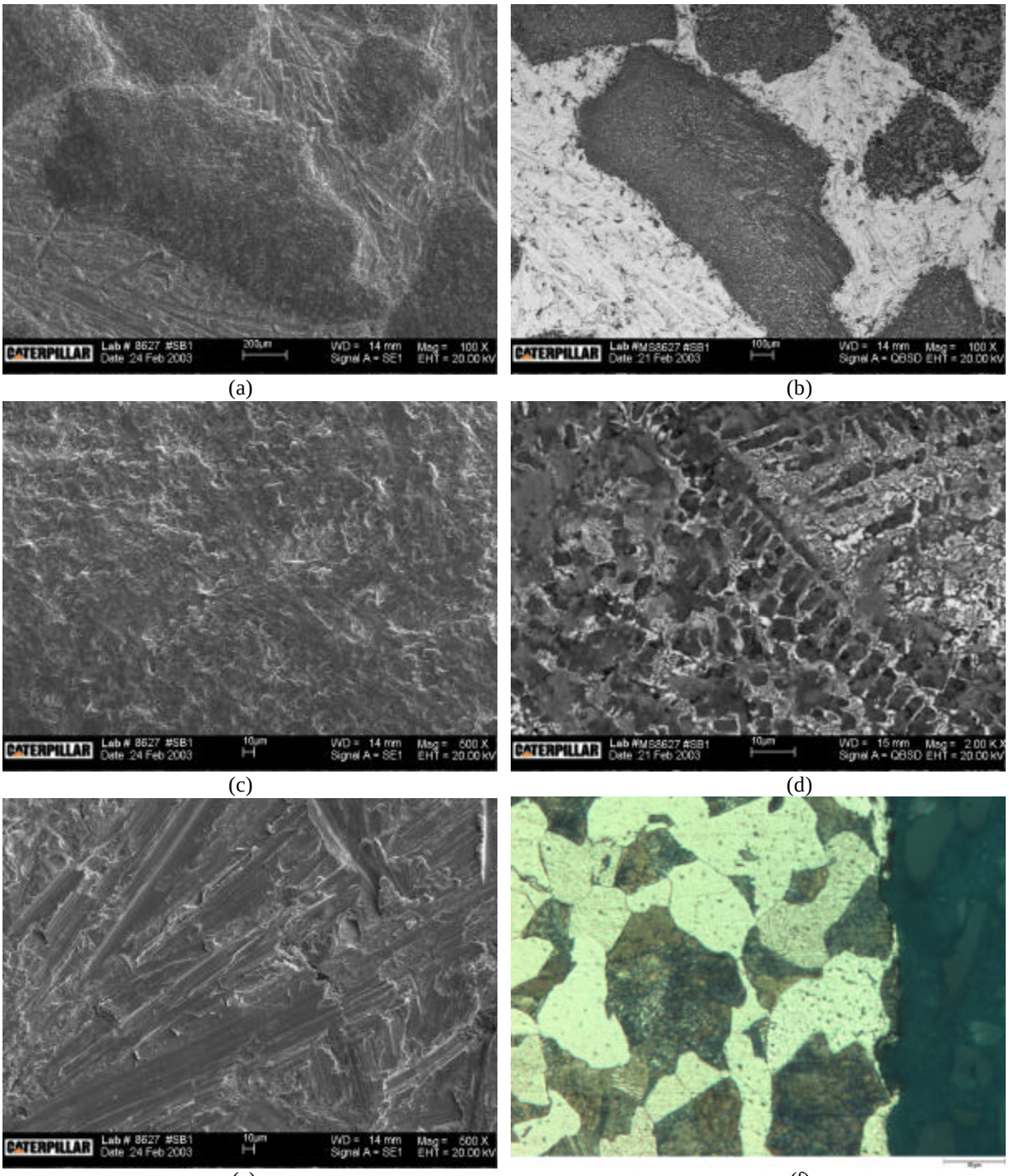

Fig. 16 Wear processes in alumina-zirconia composite where (a) and (b) show the general wear process with the hard particles (distinguishable in the backscattered SEM (b) as the darker phase) providing significant protection to the matrix. The hard particles do not show any evidence of scratches/gouges (c). The particles appear to be wearing through microfracture and grain plucking (d). The matrix shows evidence of gouging wear and plasticity (e,f), with the gouges shallower than those in the neat matrix due to the protection provided by the hard particles.

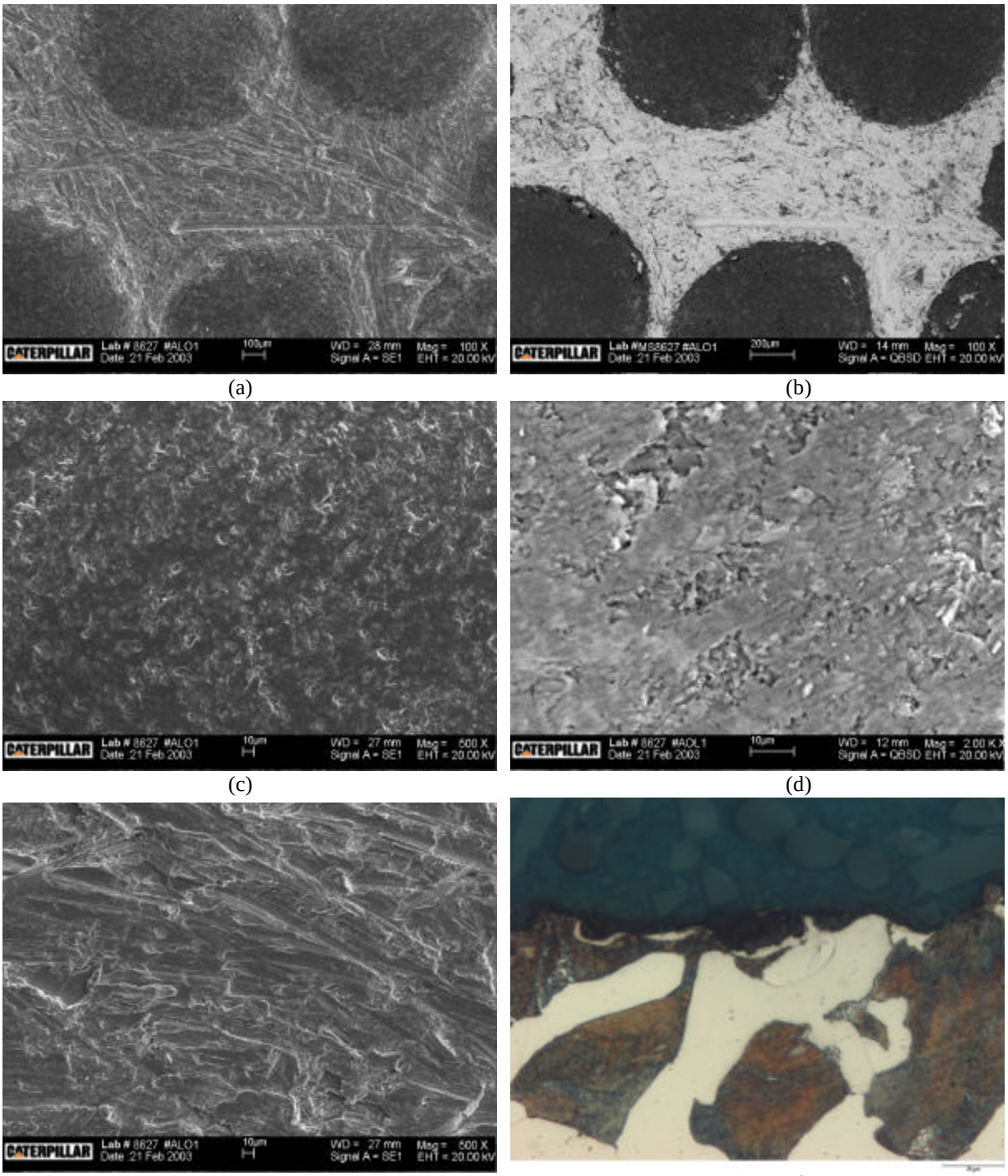

Fig. 17 Wear processes in the alumina reinforced composite where (a) and (b) show the general wear process with the hard particles (distinguishable in the backscattered SEM (b) as the darker phase) providing significant protection to the matrix. The hard particles do not show any evidence of scratches/gouges (c). The particles appear to be wearing through microfracture and grain plucking, possibly aided by small scale plasticity (d). The matrix shows evidence of gouging wear and plasticity (e,f), with the gouges shallower than those in the neat matrix due to the protection provided by the hard particles.

Conclusions and Future Work

Steel Matrix Composites

The results indicate that the present strategies for inhibiting dissolution of the WC/Co particles into the steel are ineffective. In addition, measures taken in an effort to inhibit dissolution are further reducing the toughness of the matrix in the WC/Co composites The alumina and alumina-zirconia composites appear to be immune from this problem. Among the latter two, the one containing the alumina-zirconia particles provides a superior combination of properties. It emerges as the leading candidate system for use in abrasion resistant steel components, provided a viable manufacturing route can be identified in future studies.

Thermal Spray Coatings

Laboratory wear tests will be performed with these fused coatings during the upcoming quarter. Wear rates for both the coatings and mating steel components will be determined. At the conclusion of these wear tests, destructive analyses of the fused coatings will be performed in order to determine the soundness of the metallurgical bond between the coating and substrate.

References:

No publications or documents were used or cited in the preparation of this particular quarterly report.